ELECTRONIC SUPPLEMETARY INFORMATION

Chemically Dual-Site Capture of NH_3 by Unprecedently Low-Viscous Deep Eutectic Solvents

Wen-Jing Jiang,[a] Fu-Yu Zhong,[a] Lin-Sen Zhou,[b] Hai-Long Peng,[a] Jie-Ping Fan[a] and Kuan Huang[a]*

[a]Key Laboratory of Poyang Lake Environment and Resource Utilization of Ministry of Education, School of Resources Environmental and Chemical Engineering, Nanchang University, Nanchang, Jiangxi 330031, China.

[b]Institute of Materials, China Academy of Engineering Physics, Jiangyou, Sichuan 621908, China.

*Corresponding author: huangk@ncu.edu.cn (K. H.).

EXPERIMENTAL

Materials

NH_3 (99.99 mol%) and CO_2 (99.99 mol%) were supplied by Huasheng Co. Ltd., China. Ethylamine chloride (EaCl, 98 wt.%) and phenol (PhOH, 99 wt.%) were purchased from Adamas Co. Ltd., China. All the chemicals were used directly without further purification. To prepare EaCl+PhOH DESs, the mixtures of EaCl and PhOH were stirred at 333.2 K until they became transparent liquids. The prepared DESs are denoted as EaCl+PhOH (*a*:*b*), where *a*:*b* is the molar ratio of EaCl to PhOH.

Characterizations

The water contents were measured by Karl-Fischer titration on a Titan TKF-1B analyzer with a relative uncertainty of 0.03. The densities were collected on an Anton Paar DMA 4500M densiometer with a standard uncertainty of 0.00005 g/cm^3. The viscosities were collected on a Brookfield RVDV2PCP230 viscometer with a relative uncertainty of 0.01. The thermogravimetric analysis (TGA) was conducted on a Netzsch STA 2500 analyzer at a heating rate of 5 K/min under flowing N_2 atmosphere. The ^{1}H NMR spectra were collected on an Agilent 400MR DD2 spectrometer using d_6-DMSO as the external solvent and TMS as standard.

Gas absorption measurements

The apparatus for gas absorption measurements has been reported in our previous work, and its reliability has also been verified[1]. It has two stainless steel chambers: one is used as the storage chamber and the other as the absorption chamber. The absorption chamber is equipped with a magnetic stirrer, to minimize the barrier for gas

diffusion in liquid phase. The temperature of whole apparatus is adjusted by a water bath with a standard uncertainty of 0.1 K. The pressures of two chambers are monitored by two Wideplus-8 transducers with a standard uncertainty of 1.2 kPa.

To measure the gas absorption rates, a specific amount of liquid solvent (w_L, in g) was loaded in the absorption chamber. The amount of liquid solvent was accurately weighted by an analytic balance with a standard uncertainty of 0.0001 g. Then, the whole apparatus was completely evacuated, and the gas from cylinder was loaded in the storage chamber to a pressure of P_1. The needle valve connecting two chambers was turned on to introduce a specific amount of gas into the absorption chamber, the pressure of which increased to an initial value of P_2. The pressure of storage chamber thus decreased to a value of $P_1^{'}$, and the absorption of gas in liquid solvent resulted in the decrease of P_2. The values of P_2 were recorded online, and the amount of gas absorbed at any time (m_G, in mol/kg) was calculated by the following equation:

$$m_G = [\rho_G^{P_1,T} V_1 - \rho_G^{P_1^{'},T} V_1 - \rho_G^{P_2,T} (V_2 - w_L / \rho_L)] / w_L \qquad (1)$$

where $\rho_G^{P,T}$ (in mol/cm^3) is the density of gas at the pressure of P and temperature of T; ρ_L (in g/cm^3) is the density of liquid solvent; V_1 and V_2 (in cm^3) are the volumes of storage and absorption chambers respectively. The values of $\rho_G^{P,T}$ were acquired from the NIST Chemistry WebBook[2]. The values of ρ_L were experimentally measured in this work. The values of V_1 and V_2 were also experimentally measured in this work by using helium as the probing gas. The gas absorption rates were evaluated by plotting the amounts of gas absorbed versus the absorption time.

To measure the gas absorption capacities, the absorption of gas in solvent was allowed to procced till equilibrium. When the values of P_2 remained unchanged for 1 h, the absorption of gas was considered to reach equilibrium. The amounts of gas absorbed at equilibrium condition were used as the gas absorption capacities. The capacities of gas absorption at elevated pressures were obtained by introducing more gas into the absorption chamber. The standard uncertainties of gas absorption capacities were estimated from the standard uncertainties of pressures through error propagation, since the respective contributions of the uncertainties of temperatures, volumes, mass and densities to the uncertainties of gas absorption capacities can be ignored[1].

Molecular dynamics simulations

The molecular dynamics (MD) simulations were conducted based on the density functional theory (DFT) as implemented in open-source CP2K/QUICKSTEP code[3-4]. The BLYP method[5-6] at the level of triple-zeta valence polarization basis set[7] with Goedecker–Teter–Hutter (GTH) pseudopotentials[8-9] were used. The plane-wave energy cutoff was set to 400 Ry, and the dispersion interaction was included by the D3 method (BLYP-D3) developed by Grimme et al.[10]. A 12×12×12 Å cubic box containing 3 EaCl, 6 PhOH and 3 NH_3 molecules was constructed for MD simulations. The MD simulations were conducted with canonical (NVT) ensemble employing Nosé−Hoover chain thermostats with a time step of 1 fs at a finite temperature of 300 K. After the initial structure being optimized to local minimum, the first 20 ps data of MD runs were discarded to ensure the equilibrium of system, and the radial distribution

functions (RDFs) were calculated during the following production cycles of at least 70 ps.

Quantum chemistry calculations

The quantum chemistry calculations were carried out using the Gaussian 09 program[11]. All the geometries were fully optimized by the B3LYP method based on the DFT at the level of 6-31G++(d,p) basis set[12-13]. To incorporate a condensed polar environment to DESs, a polarizable continuum model (PCM)[14] with DMSO as the solvent was used. The frequency calculations were also conducted to verify the true minima of optimized geometries. For each structure, different geometries were screened to determine the most stable geometry. The calculated energies were finally corrected by zero-point energies (ZPEs).

Table S1. Water contents of DESs prepared in this work[a]

DESs	w_{H2O}
EaCl+PhOH (1:2)	0.0037±0.0001
EaCl+PhOH (1:3)	0.0052±0.0002
EaCl+PhOH (1:5)	0.0046±0.0001
EaCl+PhOH (1:7)	0.0067±0.0002

[a]w_{H2O} is the mass fraction of water in DESs.

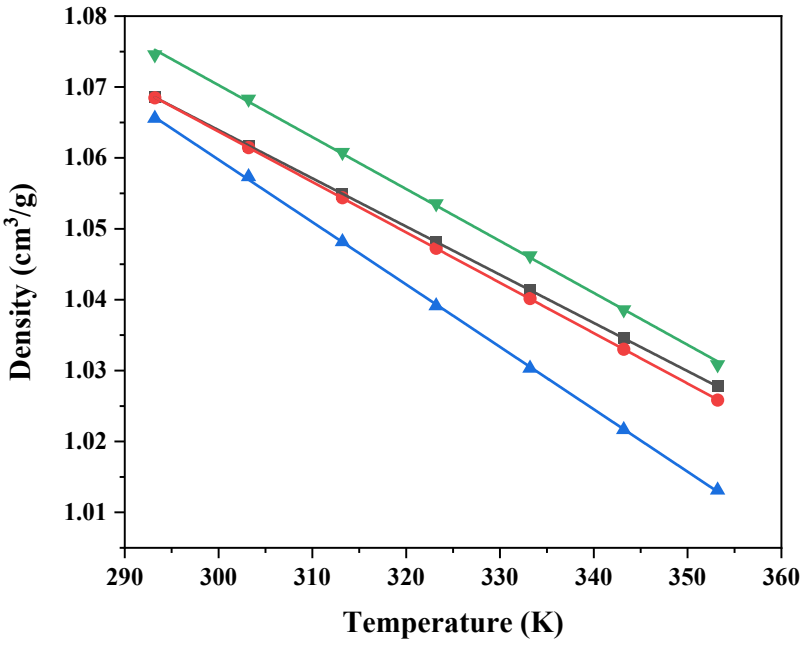

Fig. S1 Densities of EaCl+PhOH DESs [■: EaCl+PhOH (1:2), ●: EaCl+PhOH (1:3), ▲: EaCl+PhOH (1:5), ▼: EaCl+PhOH (1:7)].

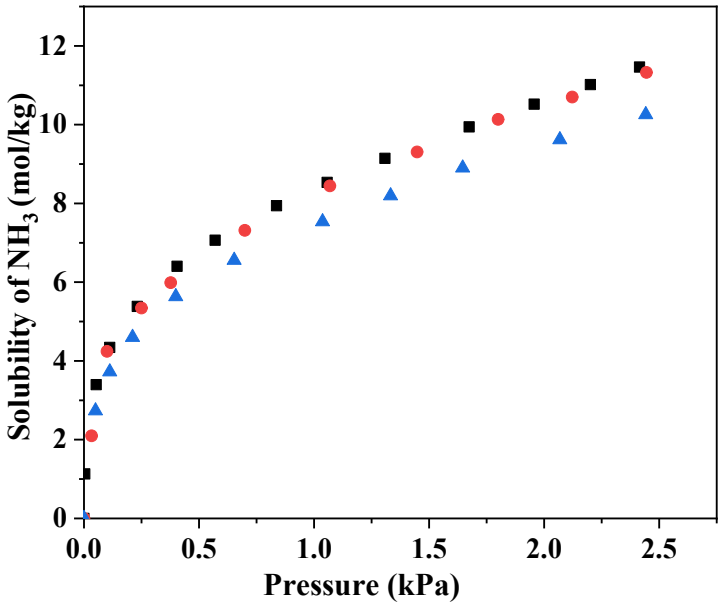

Fig. S2 Capacities of NH_3 absorption in EaCl+PhOH (1:7) with different water contents at 313.2 K (■: w_{H2O} =0.0067, ●: w_{H2O} =0.0010, ▲: w_{H2O} =0.0455).

To address the concern about water effect on NH_3 absorption, two samples of EaCl+PhOH (1:7) were further prepared: one was dried at 333.3 K and 0.1 kPa for 24 h, and the mass fraction of water was measured to be 0.0010; another was prepared by adding some water, and the mass fraction of water was measured to be 0.0455. The samples are denoted as EaCl+PhOH (1:7)-*x*, where *x* is the mass fraction of water. The NH_3 capacities of three EaCl+PhOH (1:7) samples were measured (see Fig. S2), and it is found that the NH_3 capacities of EaCl+PhOH (1:7)-0.0067 and EaCl+PhOH (1:7)-0.0010 are almost the same, and the NH_3 capacities of EaCl+PhOH (1:7)-0.0455 are only slightly lower than those of EaCl+PhOH (1:7)-0.0067.

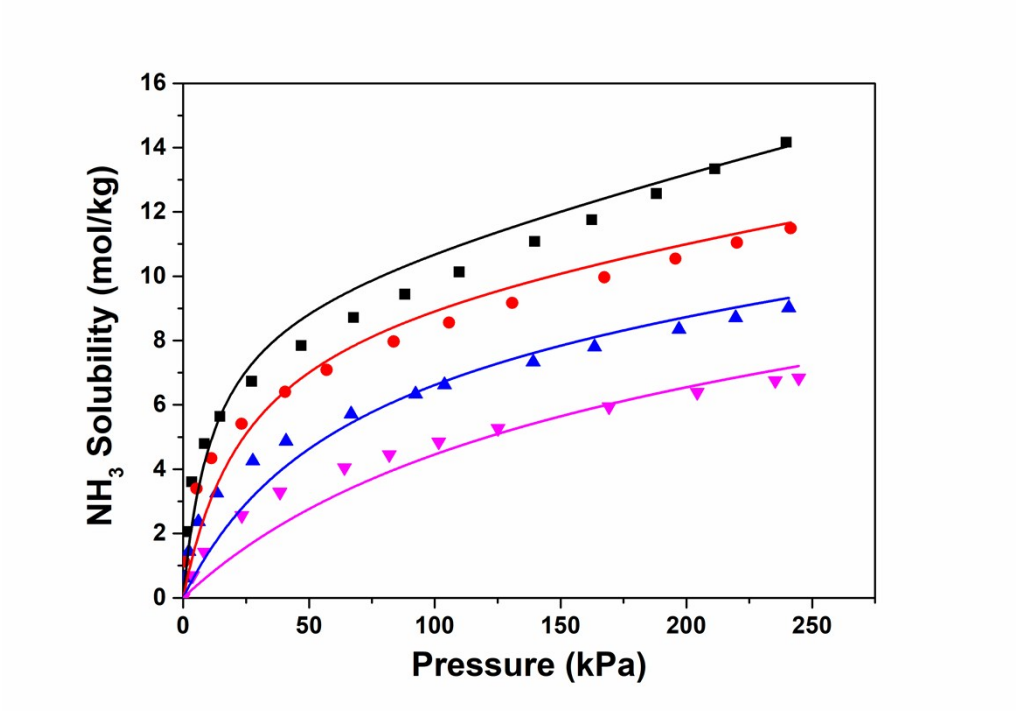

Fig. S3 Capacities of NH_3 absorption in EaCl+PhOH (1:7) at different temperatures (■:298.2 K, ●: 313.2 K, ▲: 333.2 K, ▼: 353.2 K, lines: fitting results).

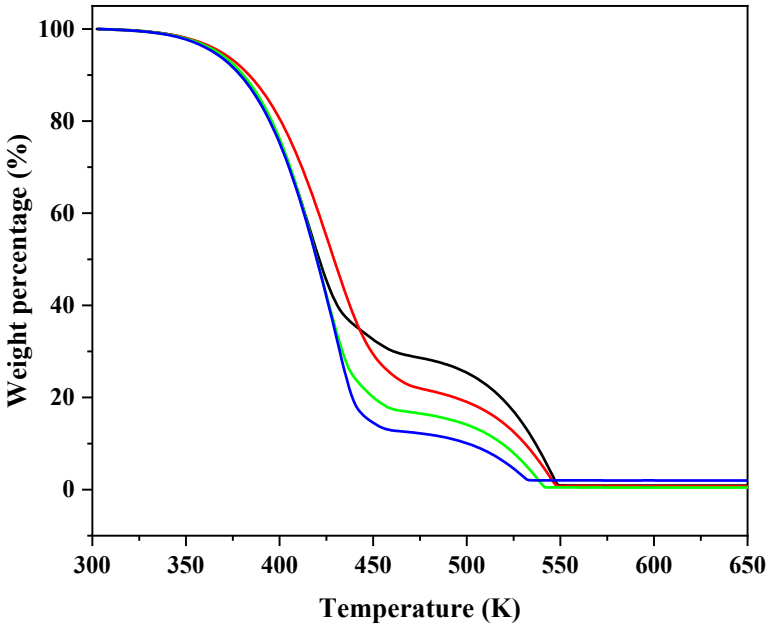

Fig. S4 TGA curves for EaCl+PhOH DESs. [black: EaCl+PhOH (1:2), red: EaCl+ PhOH (1:3), green: EaCl+ PhOH (1:5), blue: EaCl+ PhOH (1:7)]

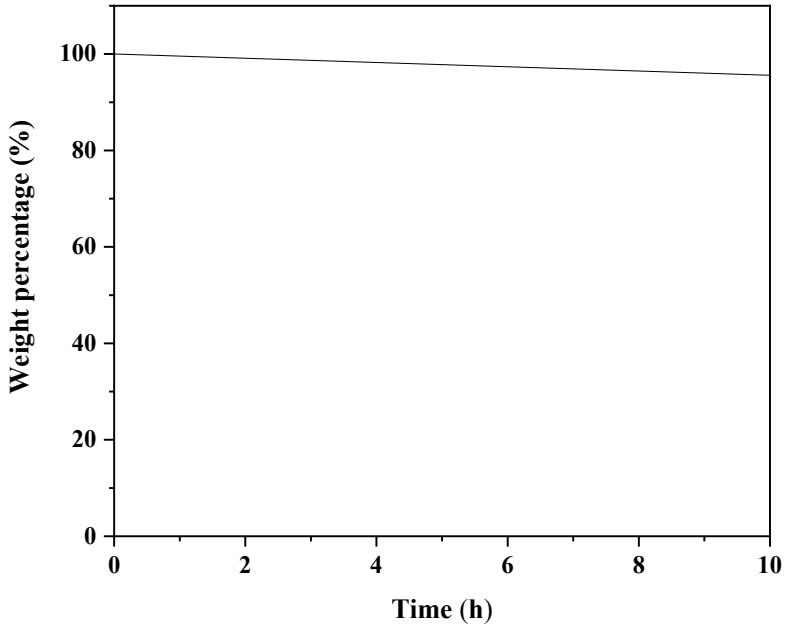

Fig. S5 Weight change of EaCl+PhOH (1:7) under N_2 purge at 333.2 K.

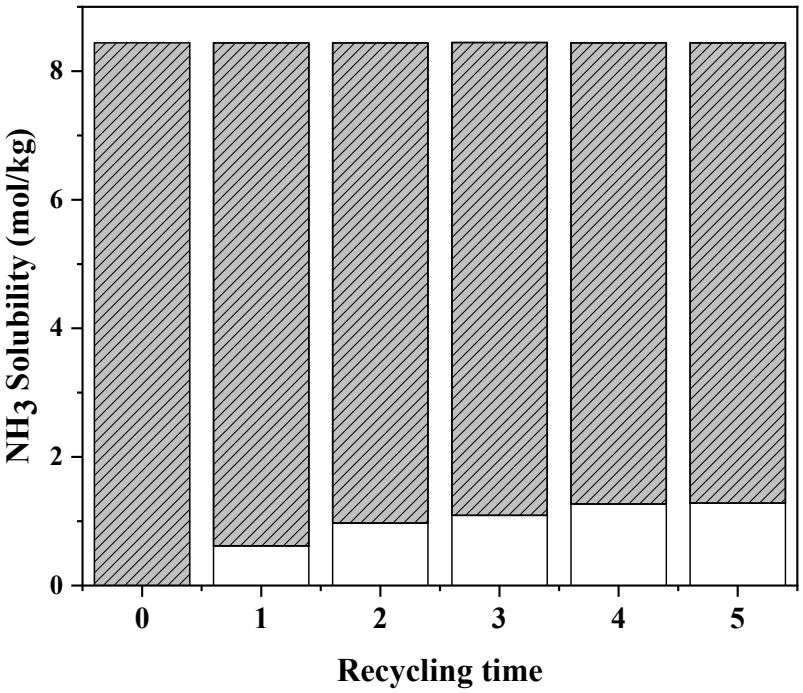

Fig. S6 Recycling of EaCl+PhOH (1:7) for NH_3 absorption (absorption condition: 313.2 K and ~100 kPa, desorption condition: 333.2 K and ~0.1 kPa).

Table S2. Comparison for NH_3 capacities of different DESs and ILs

Solvent	T (K)	P (kPa)	m_{NH3} (mol/kg)	Refs.
EaCl+PhOH (1:2)	313.2	101.3	7.023	This work
		10.0	3.443	
EaCl+PhOH (1:3)	313.2	101.3	7.433	This work
		10.0	3.709	
EaCl+PhOH (1:5)	313.2	101.3	8.106	This work
		10.0	3.881	
EaCl+PhOH (1:7)	298.2	101.3	9.801	This work
		10.0	4.991	
ChCl+Res+Gly (1:3:5)	298.2	101.3	9.982	[22]
ChCl+PhOH+EG (1:5:4)	298.2	101.3	9.619	[24]
		10.0	2.630	
NH_4SCN+Gly (2:3)	313.2	101.3	10.353	[23]
		10.0	2.391	
EaCl+Gly (1:2)	298.2	101.3	9.342	[25]
		10.0	1.588	
EaCl+AA (1:1)	313.2	101.3	3.998	[26]
		10.0	0.627	
EaCl+urea (1:1)	313.2	101.3	4.521	[27]
		10.0	0.609	
ChCl+TetrZ+EG (3:7:14)	298.2	101.3	13.687	[28]
		10.0	6.786	
[Bmim][BF_4]	298.2	101.3	0.998	[10]
[Bmim][PF_6]	298.2	101.3	1.233	[10]
[Bmim][Tf_2N]	299.4	101.3	0.311	[10]
[Bmmim][DCA]	303.0	101.3	1.139	[38]
[Emim][Ac]	298.3	101.3	1.879	[11]
[Hmim][Cl]	297.8	101.3	1.409	[10]
[EtOHmim][BF_4]	313.2	101.3	2.642	[12]
[TMGH][BF_4]	293.2	101.3	5.285	[39]
[DMEA][Ac]	298.1	101.3	5.872	[11]
[Bim][Tf_2N]	313.2	101.3	6.903	[15]
		10.0	1.297	
[Bim][SCN]	303.0	101.3	13.633	[38]
		10.0	2.12	
[Bim][NO_3]	303.0	101.3	8.465	[38]
[Mim][Tf_2N]	313.2	101.3	7.508	[38]
		101.3	3.079	
$[Emim]_2[Co(NCS)_4]$	303.2	101.3	10.726	[18]
		10.0	3.059	
$[Bmim]_2[SnCl_4]$	303.2	101.3	6.435	[19]
		10.0	1.149	

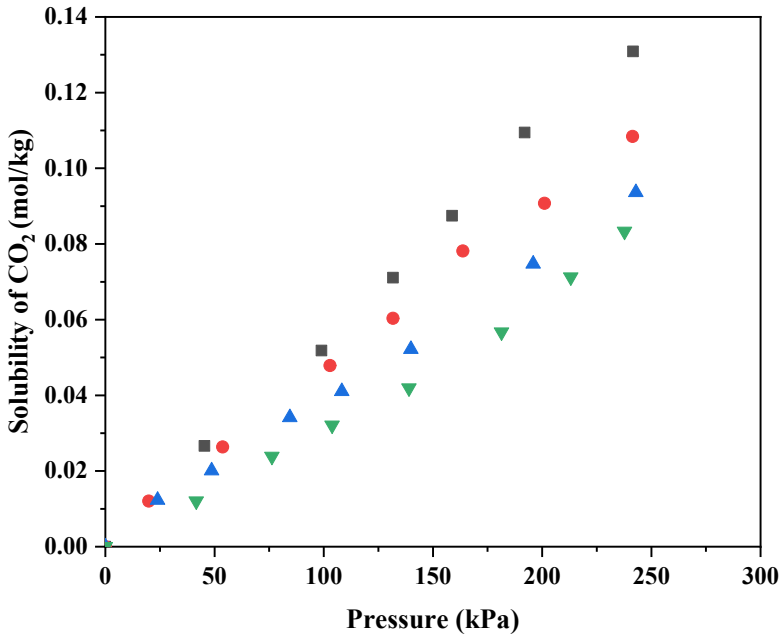

Fig. S7 Capacities of CO_2 absorption in EaCl+PhOH (1:7) at different temperatures (■: 298.2 K, ●: 313.2 K, ▲: 333.2 K, ▼: 353.2 K).

In the industrial streams, there is usually CO_2 coexisting with NH_3. Therefore, the ability of liquid solvents for the selective absorption of NH_3 from CO_2 is very important. To this end, the capacities of CO_2 absorption in EaCl+PhOH (1:7) at different temperatures were also measured (see Fig. S7). It is found that the CO_2 capacities of EaCl+PhOH (1:7) are in the range of 0.032~0.052 mol/kg at 298.2~353.2 K and 100.0 kPa, being two magnitudes lower than the NH_3 capacities. The ideal NH_3/CO_2 selectivities (defined as the ratio of NH_3 solubility to CO_2 solubility at 100.0 kPa) were calculated to be 151~195 at 298.2~353.2 K, suggesting the excellent ability of EaCl+PhOH DESs for the selective absorption of NH_3 from CO_2.

Thermodynamic calculations

Based on the experimental results, it is assumed that there are three changes for the absorption of NH_3 in EaCl+PhOH DESs: (1) NH_3 transfers from the gas phase to liquid phase; (2) EaCl reacts with NH_3 to form EaCl-NH_3 complex; (3) PhOH reacts with NH_3 to form the PhOH-NH_3 complex. The three changes can be depicted by the following expressions:

$$NH_3\ (g) \rightarrow NH_3\ (l) \qquad (4)$$

$$EaCl\ (l) + NH_3\ (g) \rightarrow EaCl\text{-}NH_3\ (l) \qquad (5)$$

$$PhOH\ (l)\ + NH_3\ (g) \rightarrow PhOH\text{-}NH_3\ (l) \qquad (6)$$

The first change is actually a physical absorption process, and can be depicted by the Henry's law equation:

$$H_{NH_3} = \frac{P_{NH_3}}{m_{NH_3}} \qquad (7)$$

where H_{NH_3} is the Henry's constant of NH_3 in liquid phase; P_{NH_3} is the pressure of NH_3 in gas phase; m_{NH_3} is the molality of free NH_3 in liquid phase. The second and third changes are actually chemical reaction processes, and can be depicted by the reaction equilibrium equations:

$$K_{EaCl} = \frac{m_{EaCl\text{-}NH_3}}{m_{EaCl} \cdot P_{NH_3}} \qquad (8)$$

$$K_{PhOH} = \frac{m_{PhOH\text{-}NH_3}}{m_{PhOH} \cdot P_{NH_3}} \qquad (9)$$

where K_{EaCl} and K_{PhOH} are the equilibrium constants for chemical reaction of EaCl with NH_3 and chemical reaction of PhOH with NH_3 respectively; $m_{EaCl\text{-}NH_3}$, m_{EaCl}, $m_{PhOH\text{-}NH_3}$ and m_{PhOH} are the molalities of EaCl-NH_3 complex, free EaCl, PhOH-NH_3

complex and free PhOH in liquid phase respectively. The mass balance equation for NH_3 is:

$$m_{NH_3}^{t} = m_{NH_3} + m_{EaCl\text{-}NH_3} + m_{PhOH\text{-}NH_3} \qquad (10)$$

where $m_{NH_3}^{t}$ is the total capacity of NH_3 absorption in DESs. The mass balance equation for EaCl and PhOH are:

$$m_{EaCl}^{0} = m_{EaCl} + m_{EaCl\text{-}NH_3} \qquad (11)$$

$$m_{PhOH}^{0} = m_{PhOH} + m_{PhOH\text{-}NH_3} \qquad (12)$$

where m_{EaCl}^{0} and m_{PhOH}^{0} are the initial molalities of EaCl and PhOH in DESs. Based on equations 7~12, the following equations can be derived:

$$m_{NH_3} = \frac{P_{NH_3}}{H_{NH_3}} \qquad (13)$$

$$m_{EaCl\text{-}NH_3} = \frac{K_{EaCl} \cdot P_{NH_3} \cdot m_{EaCl}^{0}}{K_{EaCl} \cdot P_{NH_3} + 1} \qquad (14)$$

$$m_{PhOH\text{-}NH_3} = \frac{K_{PhOH} \cdot P_{NH_3} \cdot m_{PhOH}^{0}}{K_{PhOH} \cdot P_{NH_3} + 1} \qquad (15)$$

$$m_{NH_3}^{t} = \frac{P_{NH_3}}{H_{NH_3}} + \frac{K_{EaCl} \cdot P_{NH_3} \cdot m_{EaCl}^{0}}{K_{EaCl} \cdot P_{NH_3} + 1} + \frac{K_{PhOH} \cdot P_{NH_3} \cdot m_{PhOH}^{0}}{K_{PhOH} \cdot P_{NH_3} + 1} \qquad (16)$$

Equations 13 gives the amount of NH_3 physically absorbed in liquid phase. Equation 14 gives the amount of NH_3 chemically reacting with EaCl. Equation 15 gives the amount of NH_3 chemically reacting with PhOH. Equation 16 gives the total capacity of NH_3 absorption in DESs, and is called the dual-site reaction equilibrium thermodynamic model (DS-RETM) equation.

With the Henry's constants and reaction equilibrium constants at different temperatures, the enthalpy changes for NH_3 absorption in EaCl+PhOH (1:7) can be calculated using the following equations through drawing linear fits:

$$\Delta H_{\text{phys}} = R \frac{\partial \ln H_{\text{NH}_3}}{\partial (1/T)} \qquad (17)$$

$$\Delta H_{\text{EaCl}} = -R \frac{\partial \ln K_{\text{EaCl}}}{\partial (1/T)} \qquad (18)$$

$$\Delta H_{\text{PhOH}} = -R \frac{\partial \ln K_{\text{PhOH}}}{\partial (1/T)} \qquad (19)$$

where ΔH_{phys} is the enthalpy change for physical absorption of NH_3 in EaCl+PhOH (1:7); ΔH_{EaCl} and ΔH_{PhOH} are the enthalpy changes for chemical reaction of EaCl with NH_3 and chemical reaction of PhOH with NH_3 respectively; R is the gas constant (8.314 J/mol·K). Figs. S8 and S9 show the linear fits for $\ln H_{\text{NH}_3}$, $\ln K_{\text{EaCl}}$ and $\ln K_{\text{PhOH}}$ to $1/T$.

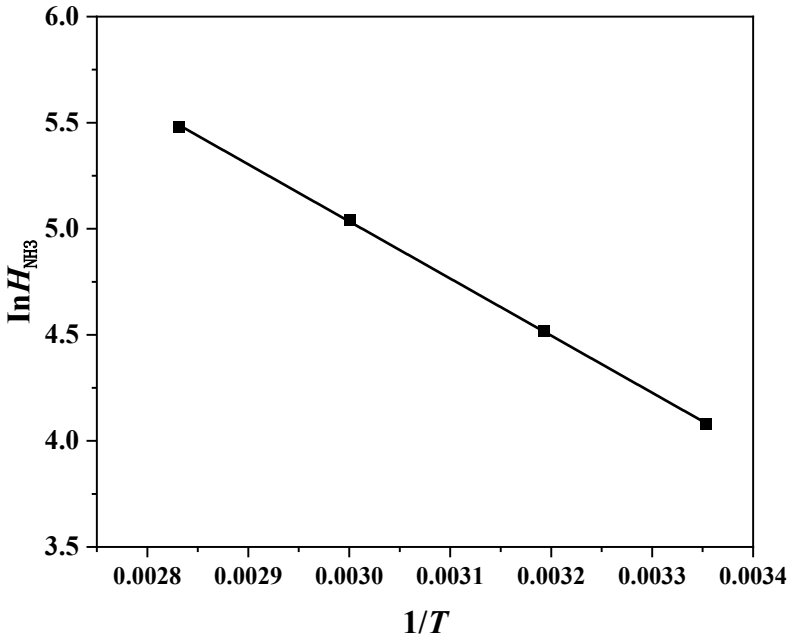

Fig. S8. Linear fits for $\ln H_{NH_3}$ to $1/T$.

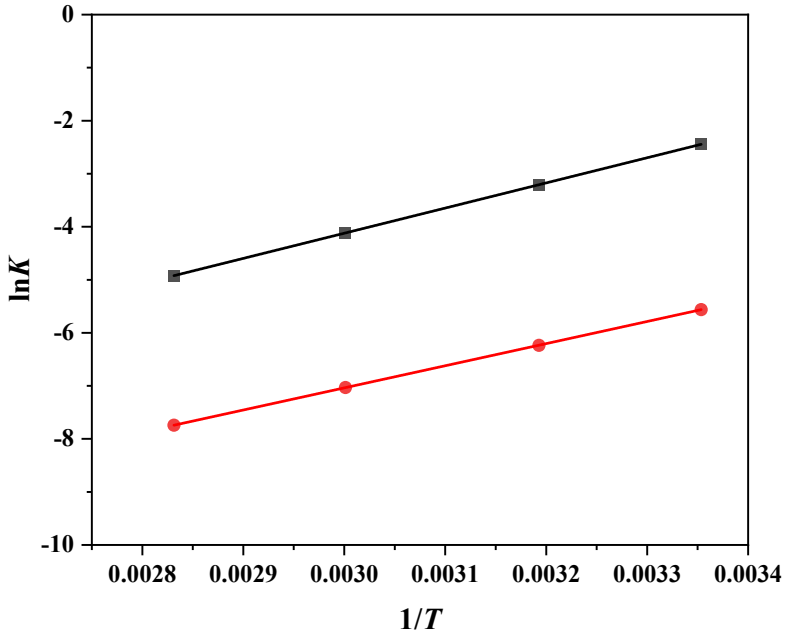

Fig. S9 Linear fits for $\ln K_{\mathrm{PhOH}}$ and $\ln K_{\mathrm{EaCl}}$ to $1/T$ (■: $\ln K_{\mathrm{PhOH}}$, ●: $\ln K_{\mathrm{EaCl}}$).

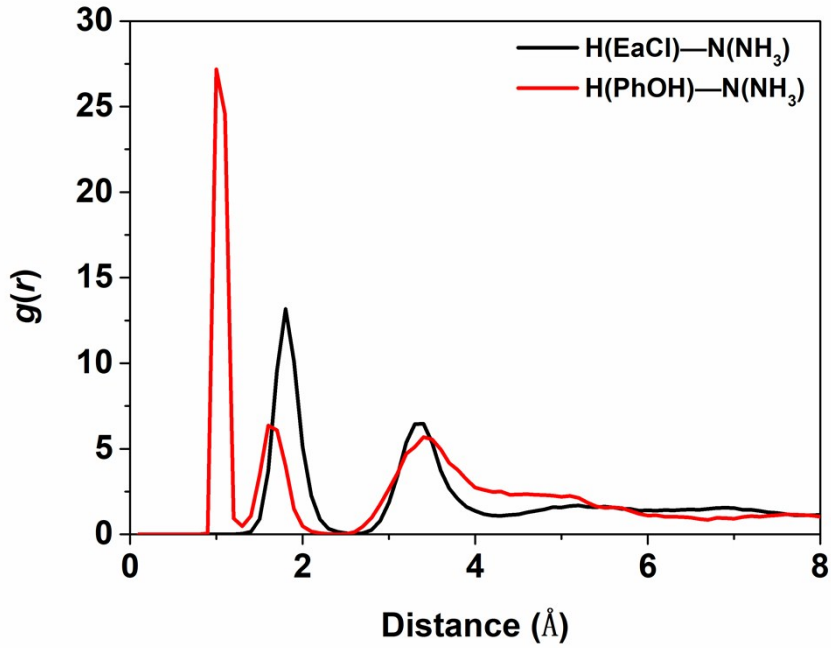

Fig. S10 Atom−atom RDFs of EaCl+PhOH+NH_3 system.

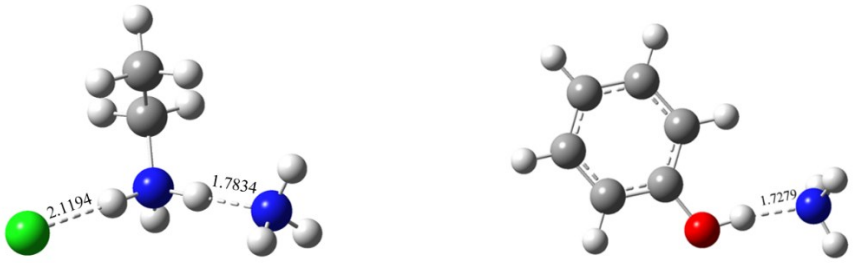

EaCl+NH_3 (ΔH=−45.0 kJ/mol) **PhOH+NH_3 (ΔH=−46.6 kJ/mol)**

Fig. S11 Optimized structures for EaCl+NH_3 and PhOH+NH_3 systems.

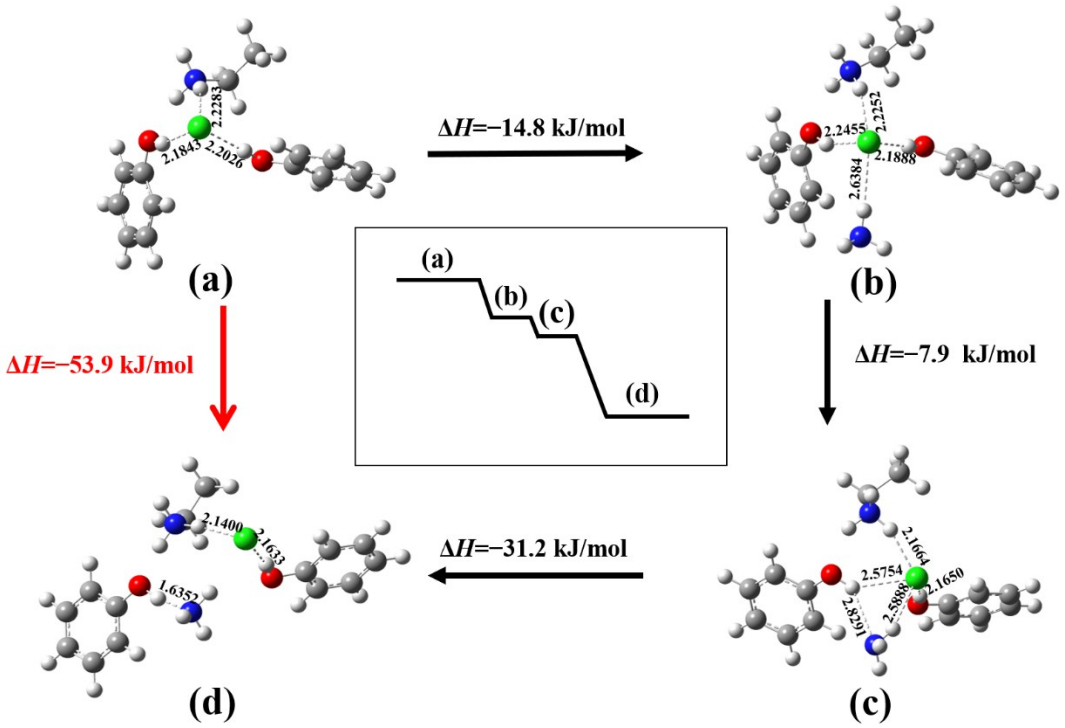

Fig. S12 Change route for interaction between acidic proton of PhOH and basic nitrogen of NH_3 in EaCl+2PhOH+NH_3 system.

In the first step, the active proton of NH_3 attaches to the chloride of EaCl to form a hydrogen bond. In the second step, the basic nitrogen of NH_3 then attaches to the acidic proton of PhOH form an intermediate geometry. In the third step, the intermolecular hydrogen bond between chloride of EaCl and acidic proton of PhOH is broken to form the most stable geometry. The enthalpy changes for three steps are −14.8, −7.9 and −31.2 kJ/mol respectively, suggesting that all the three steps are thermodynamically favorable.

References

1. F. Y. Zhong, K. Huang and H. L. Peng, *J. Chem. Thermodyn*., 2019, **129**, 5-11.
2. E. W. Lemmon, M. O. McLinden and D. G. Friend, *NIST ChemistryWebBook, NIST Standard Reference Database Number 69*, 2018, National Institute of Standards and Technology.
3. J. VandeVondele, M. Krack, F. Mohamed, M. Parrinello, T. Chassaing and J. Hutter, *Comput. Phys. Commun.*, 2005, **167**, 103-128.
4. J. Hutter, M. Iannuzzi, F. Schiffmann and J. VandeVondele, *WIREs Comput. Mol. Sci.*, 2014, **4**, 15-25.
5. A. Becke, *Phys. Rev. A*, 1988, **38**, 3098-3100.
6. C. Lee, W. Yang and R. G. Parr, *Phys Rev B: Condens Matter*, 1988, **37**, 785-789.
7. J. VandeVondele and J. Hutter, *J. Chem. Phys*., 2007, **127**, 114105.
8. C. Hartwigsen, S. Goedecker and J. Hutter, *Phys. Rev. B*, 1998, **58**, 3641-3662.
9. S. Goedecker, M. Teter and J. Hutter, *Phys Rev B Condens Matter*, 1996, **54**, 1703-1710.
10. S. Grimme, J. Antony, S. Ehrlich and H. Krieg, *J. Chem. Phys.*, 2010, **132**, 154104.
11. Frisch MJ, Trucks GW, Schlege HB, et al. *Gaussian 09*. Gaussian, Wallingford, CT, USA, 2009.
12. A. D. Becke, *J. Chem. Phys*. 1993, **98**, 5648-5652.
13. P. J. Stephens, F. J. Devlin, C. F. Chabalowski and M. J. Frisch, *J. Phys. Chem.*, 1994, **45**, 11623-11627.
14. M. Cossi, V. Barone, R. Cammi and J. Tomasi, *Chem. Phys. Lett.*, 1996, **255**, 327-335.